VIBRATION MODIFICATION IN AN OPTO-DYNAMICAL TEST SETUP FOR SUPPRESSING ABERRATIONS

Nicolai Wengert, Peter Eberhard

Institute of Engineering and Computational Mechanics
University of Stuttgart, Germany
{nicolai.wengert, peter.eberhard}@itm.uni-stuttgart.de

Keywords: Opto-dynamics, Experimental Setup, Optimization.

Abstract. *In this paper, a method is proposed for optimizing the opto-dynamical behavior of projection lenses. This method is an alternative to using active and passive damping which is both limited in high-performance optical systems. The core of the optimization is a reliable prediction of the input-output behavior. Simulations and optimizations are verified by experiments involving a test objective with modifiable mechanical supports of the optical elements. The individual bodies of the test objective correspond mechanically to pendula with one degree of freedom connected by springs. For modifying the dynamical behavior, stiffnesses and moments of inertia can be adjusted. By applying a well-defined excitation, the optical elements start to vibrate. This, subsequently, makes the projected image vibrate as well. The aim is to minimize this image motion to reduce the blurring of the exposure.*

1 INTRODUCTION

Vibrations are an increasing problem in optical lithography, an important step in microchip production [1]. Microchips are created on a thin silicon disc, a so-called wafer. In a wafer stepper, see Figure 1, small structures are projected onto a light resistive coating on the wafer. By means of etching, a mask is created which allows for a processing of the layer underneath the mask. Since the mask is a result of the exposed image, and its structure size is in the range of nanometers, smallest errors in the exposed image can cause broken chips. Deficient images have several error sources, e.g. the dynamical behavior of the optical components in the lithographic projection lens. Those imaging errors are so-called dynamically-induced aberrations. Vibration sources could be noise, ground vibrations, and wafer stage motion.

Avoiding vibrations of optical components is a challenging task. The main problem are the vibration amplitudes which are in the range of nanometers. This can hardly be resolved by sensors. Consequently, active vibration damping is very difficult. Furthermore, passive damping is limited due to design-related specifications. Another possibility for reducing aberrations is given in [2]. This method combines the mechanical and optical model to optimize the opto-dynamical behavior. In general, vibrations do not have to be avoided but the influence of vibrations on the image projection is to be minimized. Here, the main issue is minimizing the abberations of the individual mode shapes and, thus, minimizing aberrations in general. This can be achieved by modifying the mechanical design of a projection lens and its support structure.

The aim of this paper is to verify this method to be successful by means of experiments. First, a test objective and its periphery will be introduced. Second, modeling the mechanical part will be discussed followed by optimizing the opto-dynamical behavior. Measurements will be shown and compared to simulations. Finally, the results will be discussed.
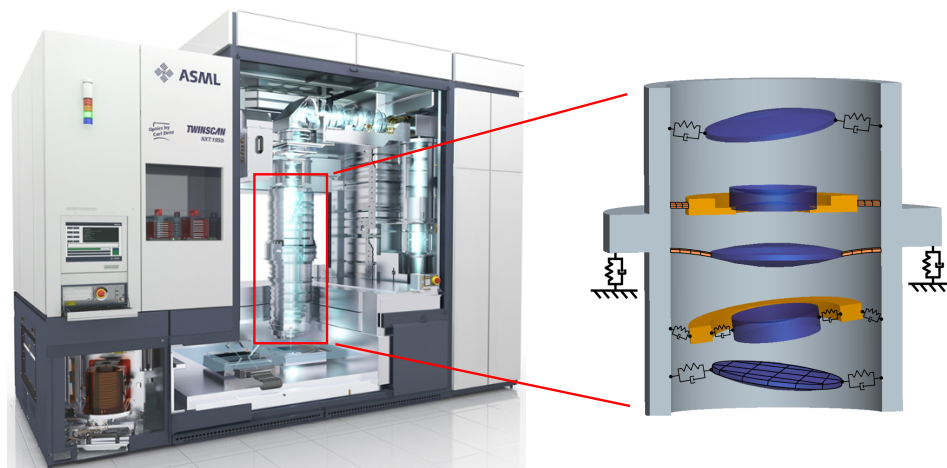

Figure 1: A wafer stepper (photo from ASML) for projecting small structures on a photo resist and a multibody model of a lithographic projection lens.

2 THE EXPERIMENTAL SETUP

A test objective has been designed and built as it can be seen in Figure 2. It is roughly derived from current lithographic projection lenses. As any ordinary optical system, it comprises a light source, an object plane, optical elements (here: six lenses), and an image plane. The object

is represented by a transparent circle, so that the image is a light point. At the image plane, a paper screen is used to make the light point visible. A high speed camera is located behind the screen for recording the moving light point. The motion of the light point is caused by vibrating lenses. The lenses are supported in pendula which are connected to other pendula by springs. This allows for vibrations with low frequencies and high amplitudes which make the motion visible for the eyes, in contrast to real objectives.
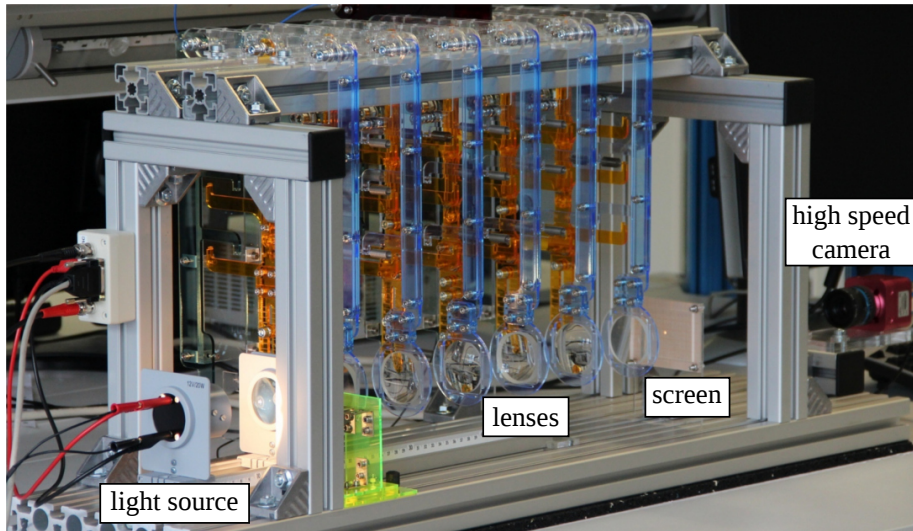

Figure 2: The experimental test setup comprising the test objective and measurement devices for both mechanics and optics.

The link between the mechanical model of the test setup and the lithographic projection lens is shown in Figure 3. Transversal motion, i.e. motion perpendicular to the optical axis, produces significantly higher aberrations than motion in other directions. Therefore, the design in Figure 3c was chosen which emulates this motion. Except for some few details, the mathematical models are the same for Figure 3b and Figure 3c.
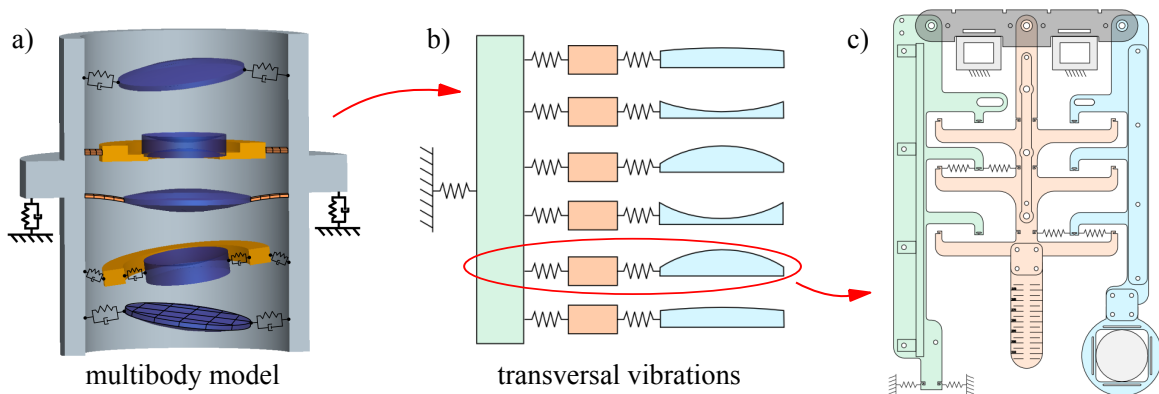

Figure 3: *a)* Multibody model of a lithographic projection lens. *b)* Simplified mechanical model for simulating transversal vibrations. *c)* A single component of the experimental setup.

The measurement setup is presented in Figure 4. An excitation performed by an impact hammer starts the measurement. The hammer is fixed to a suspension which makes sure that

the impact force is always the same. The modal analyzer controls the frame grabber which, in turn, makes the high speed camera taking pictures for recording a video. After a certain duration, the recording stops and the results can be stored on a hard disk.
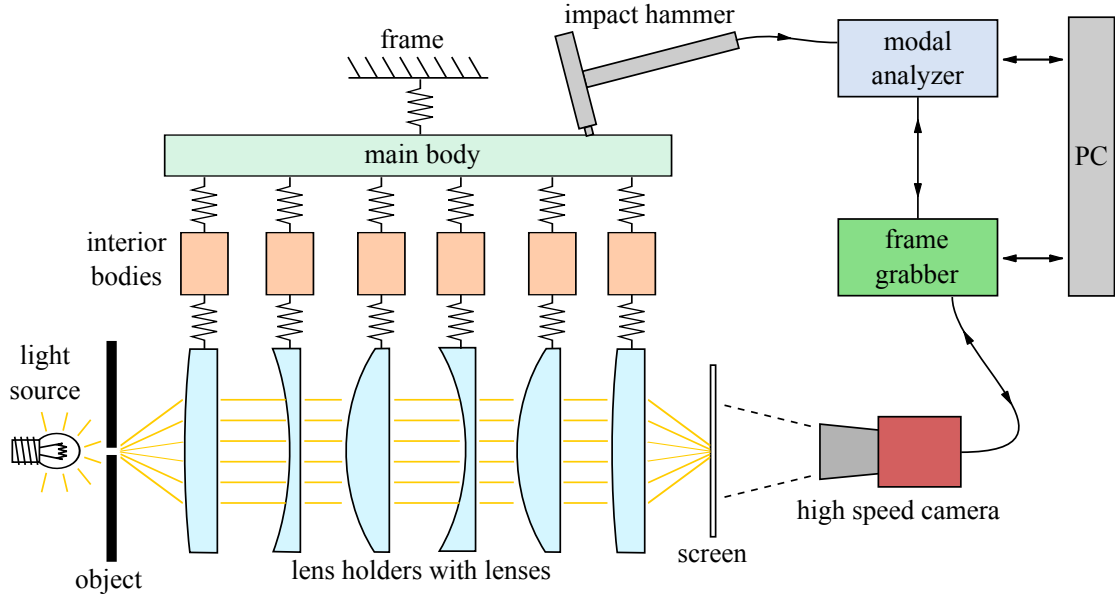

Figure 4: Principle of the measurement setup: the objective with peripheral measurement devices.

3   SIMULATION MODEL AND OPTIMIZATION

The design introduced in the previous section is now to be modeled and optimized. First, the equations of motion for two pendula will be derived. Then, the system matrices will be set up. After this, the input-output behavior of the modally transformed system will be discussed which leads to the performance function for the optimization. It should be noted that damping will be neglected in the following but can easily be added if required.

3.1   Two pendula

Stiffnesses of all connections between two pendula can be handled as described in this subsection, except from the connection between main body and frame. Figure 5 shows a component with main body, interior body, and lens holder. A certain section is taken for pointing out the assembly of the equations of motion for two pendula. All pendula are supported in such a way that they only perform rotational motion in the xy-plane.

Referring to the nomenclature in Figure 5, the equations of motion read

$$I_I\ddot{\phi}_I = (-\boldsymbol{p}_1(\phi_I) \times \boldsymbol{F}_1(\phi_I, \phi_L) + \boldsymbol{p}_3(\phi_I) \times \boldsymbol{F}_2(\phi_I, \phi_L)) \cdot \boldsymbol{e}_z + m_I g d_{sI} \sin\phi_I, \qquad (1)$$

$$I_L\ddot{\phi}_L = (-\boldsymbol{p}_2(\phi_L) \times (\boldsymbol{F}_1(\phi_I, \phi_L) - \boldsymbol{F}_2(\phi_I, \phi_L))) \cdot \boldsymbol{e}_z + m_L g d_{sL} \sin\phi_L, \qquad (2)$$

with the moments of inertia I_i, the masses m_i, the acceleration due to gravity g, and the distances d_{si} from the rotation axes to the centers of gravity. The index I names the interior body and L the lens holder with the lens. A linearization for small motion ($\sin\phi \approx \phi$, $\cos\phi \approx 1$) yields

$$\boldsymbol{M}_{IL} \cdot \begin{bmatrix} \ddot{\phi}_1 \\ \ddot{\phi}_2 \end{bmatrix} + \boldsymbol{K}_{IL} \cdot \begin{bmatrix} \phi_1 \\ \phi_2 \end{bmatrix} = \boldsymbol{0} \qquad (3)$$
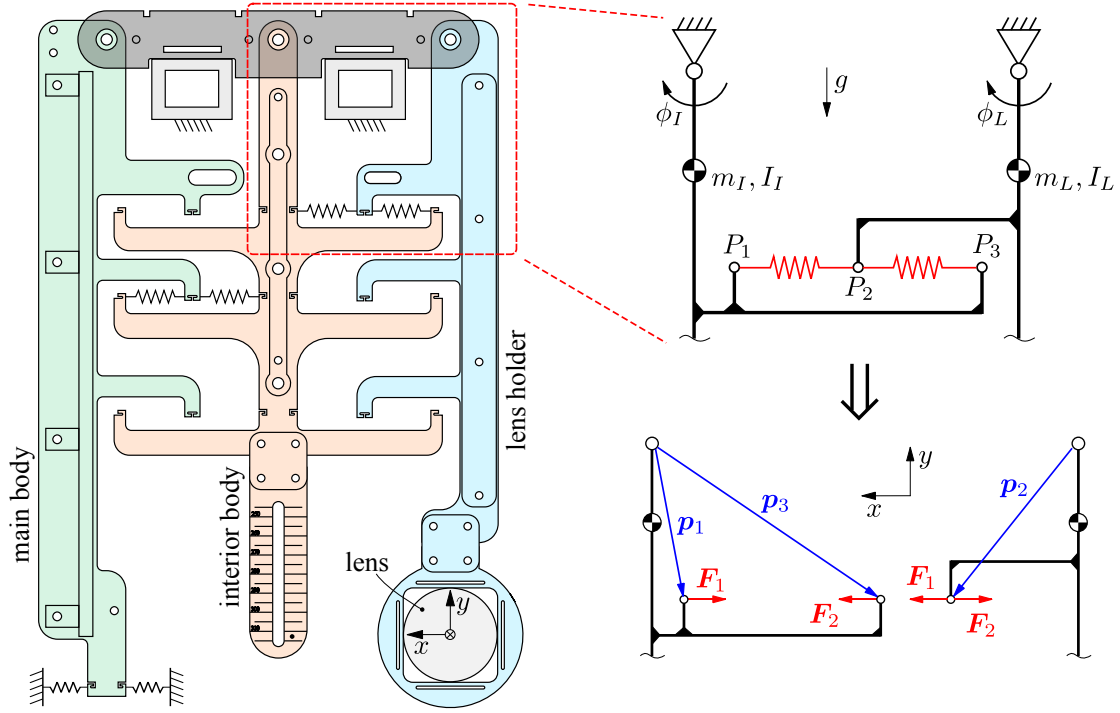
4

Figure 5: A single component and a draft for calculating the stiffnes matrix for two pendula.

with the mass matrix $\boldsymbol{M}_{IL}$ and the stiffness matrix $\boldsymbol{K}_{IL}$ for two unconstrained pendula,

$$\boldsymbol{M}_{IL} = \begin{bmatrix} I_I & 0 \\ 0 & I_L \end{bmatrix} \qquad \text{and} \qquad \boldsymbol{K}_{IL} = \begin{bmatrix} \kappa_{IL,d} + \kappa_{g,I} & -\kappa_{IL,sd} \\ -\kappa_{IL,sd} & \kappa_{IL,d} + \kappa_{g,L} \end{bmatrix}. \tag{4}$$

The diagonal elements in the stiffness matrix are separated into $\kappa_{IL,d}$, which results from the springs, and $\kappa_{g,i}$, which results from gravity.

3.2 System equations

In the test setup, all individual main bodies of the components are connected to each other by rigid plates. Thus, there is only one big main body remaining. Expanding the local model from Figure 5 to the full model leads to the global equations of motion,

$$\boldsymbol{M} \cdot \ddot{\boldsymbol{y}} + \boldsymbol{K} \cdot \boldsymbol{y} = \boldsymbol{B}\, u, \tag{5}$$

with the generalized coordinates

$$\boldsymbol{y} = [\phi_M, \ \phi_{I1}, \ \phi_{L1}, \ \dots, \ \phi_{I6}, \ \phi_{L6}]^T. \tag{6}$$

There are six components in the experimental setup. The index M denotes the main body. On the right hand side of Eq. (5), there are the input matrix

$$\boldsymbol{B} = [1, \ 0, \ 0, \ 0, \ 0, \ 0, \ 0, \ 0, \ 0, \ 0, \ 0, \ 0, \ 0]^T, \tag{7}$$

and the scalar input u. In this experiment, only a simple torque is applied to the main body by means of a hammer impulse on the pendulum.

5

So far, the mechanical motion of the test setup can be simulated. However, the optical aberration is the desired result. That is obtained using the lens sensitivities s_i in x-direction. Here, lens sensitivities are defined by

$$s_i = \frac{\text{displacement of the light point on the screen}}{\text{displacement of lens } i \text{ in } x\text{-direction}}. \tag{8}$$

Due to small rotations and the high distance between rotation axis and lenses, the motion of the lenses can be approximated to x-displacements exclusively. Considering this simplification in the output matrix, it follows

$$\boldsymbol{C}_a = [0,\ 0,\ s_1 d_L,\ 0,\ s_2 d_L,\ 0,\ s_3 d_L,\ 0,\ s_4 d_L,\ 0,\ s_5 d_L,\ 0,\ s_6 d_L] \tag{9}$$

with the distance d_L from the center of gravity of the lenses to the rotation axis. Finally, the aberrations a_{crd} (crd=chief ray deviation) can be computed by

$$a_{crd} = \boldsymbol{C}_a \cdot \boldsymbol{y}. \tag{10}$$

Here, due to the optical design, the chief ray deviation describes the displacement of the light point.

3.3 The frequency domain behavior of the projection lens

For optimizing the projection lens, the transfer function in the frequency domain of the modally transformed system is required. With this, it is possible to determine the influence of the individual modes on the light point motion, see [2] and [3].

A modal transformation requires the computation of the eigenvectors ϕ_j. The eigenvectors are summarized in the modal matrix $\boldsymbol{\Phi} = [\phi_1,\ \ldots, \phi_{n_{dof}}]$ with n_{dof} being the number of degrees of freedom. With the modal matrix, a modal transformation of Eqs. (5) and (10) can be realized. The substitution $\boldsymbol{y} = \boldsymbol{\Phi} \cdot \tilde{\boldsymbol{y}}$ and a pre-multiplication with $\boldsymbol{\Phi}^T$ yields

$$\tilde{\boldsymbol{M}} \cdot \ddot{\tilde{\boldsymbol{y}}} + \tilde{\boldsymbol{K}} \cdot \tilde{\boldsymbol{y}} = \tilde{\boldsymbol{B}}\, u \tag{11}$$

$$a_{crd} = \tilde{\boldsymbol{C}}_a \cdot \tilde{\boldsymbol{y}} \tag{12}$$

with $\tilde{\boldsymbol{M}} = \boldsymbol{\Phi}^T \cdot \boldsymbol{M} \cdot \boldsymbol{\Phi}$, $\tilde{\boldsymbol{K}} = \boldsymbol{\Phi}^T \cdot \boldsymbol{K} \cdot \boldsymbol{\Phi}$, $\tilde{\boldsymbol{B}} = \boldsymbol{\Phi}^T \cdot \boldsymbol{B}$ and $\tilde{\boldsymbol{C}}_a = \boldsymbol{C}_a \cdot \boldsymbol{\Phi}$. Scaling the eigenvectors so that $\tilde{\boldsymbol{M}} = \boldsymbol{E}$ and $\tilde{\boldsymbol{K}} = \text{diag}(\omega_j^2)$ simplifies Eq. (11). According to [4] or [5], the transfer function of this SISO (single input single output) system has the form

$$H(\omega) = \frac{\hat{a}_{crd}(\omega)}{\hat{u}(\omega)} = \sum_{j=1}^{n_{dof}} \frac{\tilde{C}_{a,j} \tilde{B}_j}{\omega_j^2 - \omega^2} \equiv \sum_{j=1}^{n_{dof}} H_j \tag{13}$$

where $\hat{a}_{crd}$ is the aberration and $\hat{u}$ the excitation in the frequency domain, and $\omega_j = 2\pi f_j$ the angular eigenfrequencies.

3.4 Minimizing the transfer function

Equation (13) demonstrates the dependency of the aberration from the excitation. The conclusion is clear: the lower the transfer function, the lower the aberration, and the better the opto-dynamical behavior of the projection lens. For doing an optimization, it is essential to

make transfer functions comparable for models with different parameters. The problem is that the transfer function diverges near eigenfrequencies,

$$\lim_{\omega \to \omega_j} |H(\omega)| = \infty. \tag{14}$$

Moreover, the area between H and the ω-axis diverges. This can be shown by the convergence criterion which is violated,

$$\lim_{\omega \to \omega_j^-} (\omega_j - \omega) H_j(\omega) = \frac{\tilde{C}_{a,j} \tilde{B}_j}{2\omega_j} \neq 0. \tag{15}$$

However, this criterion describes an amplitude of H_j. Extracting the parameter-dependent variables in the limit of Eq. (15) allows for a normalization near eigenfrequencies. Assuming $\omega_j - \omega^*$ to be small,

$$\frac{1}{w_j} H_j(\omega^*) \approx \text{const.} \qquad \text{with} \qquad w_j = \frac{|\tilde{C}_{a,j} \tilde{B}_j|}{\omega_j}. \tag{16}$$

The amplification factor w_j defines the input-ouput ratio at the eigenfrequency f_j, i.e. it quantifies the influence of a sinusoidal excitation of frequency f_j on the aberration. To review, the aim is to minimize the aberrations in the freqency domain $|\hat{a}_{crd}(\omega)| = |H(\omega)\hat{u}(\omega)|$. Minimizing the amplification factors w_j is an equivalent issue. Therefore, they can be used in the performance function and the optimization problem becomes

$$\min f(\boldsymbol{p}) \qquad \text{with} \qquad f(\boldsymbol{p}) = \sum_{j=1}^{n_{dof}} \frac{|\tilde{C}_{a,j} \tilde{B}_j|}{\omega_j} \hat{u}(\omega). \tag{17}$$

with the design parameters $\boldsymbol{p}$. In the test setup, the design parameters are the moments of inertia of the interior bodies, stiffnesses between main body and interior bodies, and stiffnesses between interior bodies and lens holders.

4 MEASUREMENT EXAMPLES

The test setup has a high flexibility regarding the modification of parameters. The moments of inertia of the interior bodies can be varied between $3.26 \cdot 10^{-3}$ and $5.89 \cdot 10^{-3}\,\text{kg}\,\text{m}^2$ continuesly. Rotational stiffnesses may vary in nine levels from 2.7 to 14.6 Nm/rad. In addition, components can be decoupled to make the model smaller, and parameters can be excluded from the optimization. Accordingly, a huge number of different parameter sets can be tested. In this section, three examples will be shown which represent the experiences of several measurements.

4.1 Lens triplet

The first example is meant to describe the way of evaluating a measurement. For a simple system, first a lens triplet is used, i.e. an objective with three lenses. Its mechanical model is presented in Figure 6 where components 1, 2, and 6 are decoupled. The numbers on the lens bodies specify the sensitivities of the lenses. The numbers on the interior bodies and on the springs represent the normalized design parameters. The lower and upper bounds for the normalized moments of inertia of the interior bodies are -10 and 10, respectively. Rotational stiffnesses are normalized from 1 to 9 which indicates the level of stiffness. An impulse hammer is used to

excite at the main body (light green). The hammer impulse provides constant amplitudes in the investigated frequency range (0...15 Hz). Thus, in the optimization, a constant value $\hat{u} = 1$ can be used. Parallel to the hammer impact, the high speed camera starts recording the deviation of the light point a_{crd}. In the ideal case, the exposured image is a white filled circle with sharp edges. In any other case, it becomes blurred. The exposure is a qualitative indicator for the opto-dynamical behavior: the more it is blurred, the worse the parameter choice.
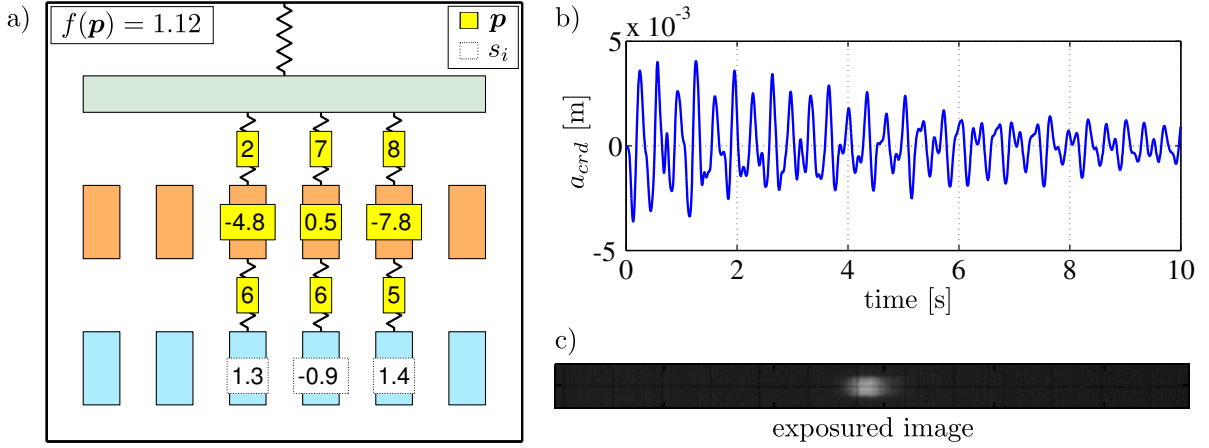
Figure 6: *a)* A draft of the mechanical model with numbers for design parameters p and sensitivities s_i. *b)* Light point motion a_{crd} recorded by the camera. *c)* The corresponding exposure.

A comparison between measurement and simulation is shown in Figure 7. The Fourier transform (FT) of the light point motion has peaks at the eigenfrequencies of the real triplet. In the lower frequency range, they correspond well to the simulated f_i. Comparing the amplitudes of the peaks to the amplification factors w_i confirms the prediction of the input-output behavior.
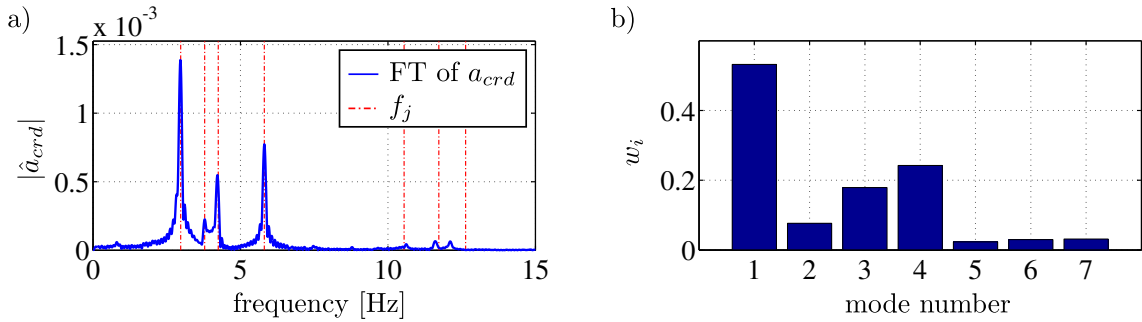

Figure 7: *a)* Fourier transform of the light point motion a_{crd} and the simulated eigenfrequencies f_j of the triplet. *b)* Amplification factors w_j of the triplet according to Eq. (16).

4.2 Application of the optimization

Next, two examples will be presented with an initial and an optimized set of parameters, see Figure 8. This time, all six components are connected to the main body. For the optimization, a genetic algorithm [6] is used since there are many local minima. In the optimized design, a relevant issue can be found at lenses 3 and 5. Those two lenses have the highest sensitivities,

and stiffnesses between lenses and interior bodies are at the upper bound, whereas stiffnesses between interior bodies and main body are at the lower bound. For lenses with negative sensitivities, it is approximately vice-versa. Moments of inertia tend to be distributed in their parameter range.
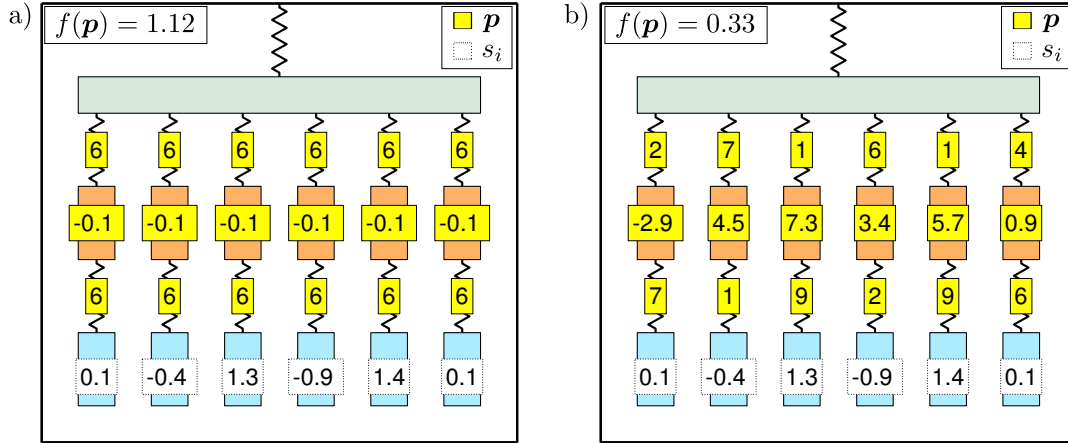

Figure 8: *a)* Initial set of parameters. *b)* A set of parameters after an optimization with a genetic algorithm.

The measured light point motion and its corresponding Fourier transform are shown in Figure 9. The aberration is significantly smaller for the optimized design. This can be observed both in the time and freqency domain. The goal was to minimize the frequency response which, in fact, was achieved.
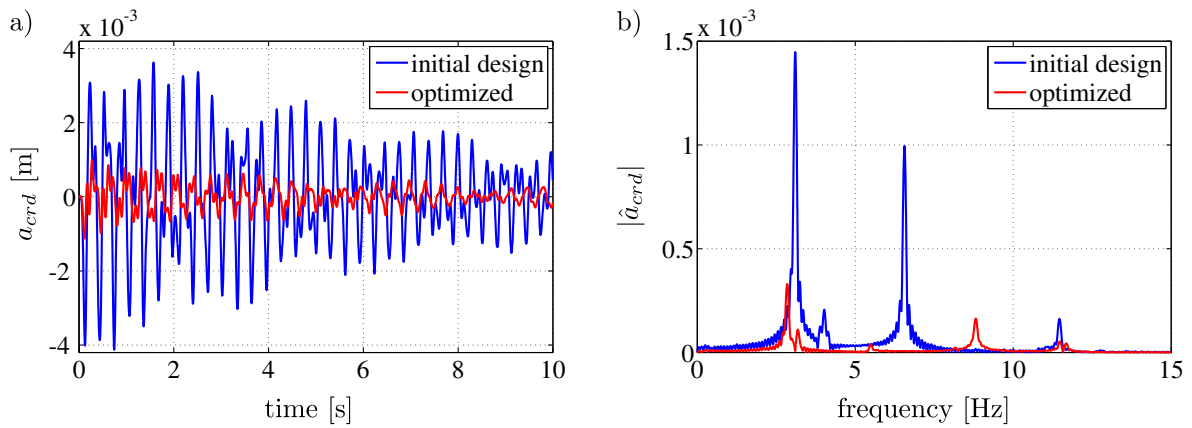

Figure 9: *a)* Light point motion after the hammer impulse. *b)* Fourier transform of a_{crd}.

Concerning lithography, the result of interest is the exposed image. The two exposures are presented in Figure 10. They are recorded during a time duration of 10 seconds starting with the hammer impulse. The exposure of the initial design is clearly blurred, whereas the exposure of the optimized design is only slightly blurred. Correspondingly, a better opto-dynamical behavior can be stated for the optimized design.
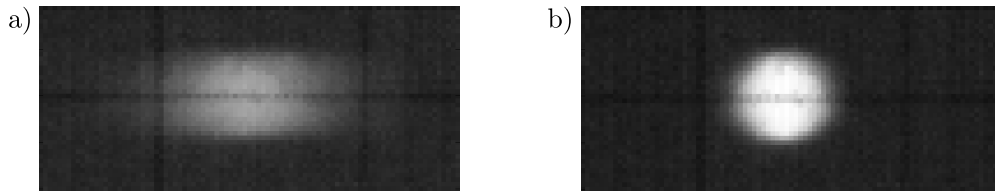
9

a) b)

Figure 10: *a)* Recorded exposure of the initial design. *b)* Recorded exposure of the optimized design.

5 CONCLUSIONS

The experiments verify the simulation and optimization methods. They succeeded to predict the influence of the excitation on the projected image by means of the amplification factors w_i. This is affirmed by the correlation between these factors and the amplitude of the peaks in the frequency spectrum of the measured aberration. Therefore, this verifies the derivation of the performance function for minimizing the aberrations for a certain excitation.

Moreover, experiences can be gained to improve real lithographic projection lenses. This especially regards stiffness distributions in components with high positive or negative optical sensitivities.

REFERENCES

[1] C. Mack, *Fundamental Principles of Optical Lithography*. John Wiley, Chichester, 2007.

[2] N. Wengert, P. Eberhard, Optimization of the Dynamical Behavior of High-performance Lens Systems to Reduce Dynamic Aberrations, *The Archive of Mechanical Engineering*, **58**, 407-423, 2011.

[3] N. Wengert, M. Nefzi, P. Eberhard, B. Geuppert, Dynamics in Lithographic Projection Objectives. *Multibody System Dynamics*, 2013 (DOI: 10.1007/s11044-013-9344-0).

[4] Z. Fu, J. He, *Modal Analysis*. Butterworth Heinemann, Oxford, 2001.

[5] F. Kollmann, T. Schösser, R. Angert, *Maschinenakustik (in German)*. Springer, Berlin, 2006.

[6] K. Deep, K.P. Singh, M.L. Kansal, C. Mohan, A Real Coded Genetic Algorithm for Solving Integer and Mixed Integer Optimization Problems, *Applied Mathematics and Computation*, **212**, 505-518, 2009.